

Saturation of elliptic flow and shear viscosity

A. K. Chaudhuri*

Variable Energy Cyclotron Centre, 1/AF, Bidhan Nagar, Kolkata 700 064, India

(Dated: January 13, 2019)

Effect of shear viscosity on elliptic flow is studied in causal dissipative hydrodynamics in 2+1 dimensions. Elliptic flow is reduced in viscous dynamics. Causal evolution of minimally viscous fluid ($\eta/s=0.08$), can explain the PHENIX data on elliptic flow in 16-23% Au+Au collisions up to $p_T \approx 3.6$ GeV. In contrast, ideal hydrodynamics, can explain the same data only up to $p_T \approx 1.5$ GeV. p_T spectra of identified particles are also better explained in minimally viscous fluid than in ideal dynamics. However, saturation of elliptic flow at large p_T is not reproduced.

PACS numbers: 47.75.+f, 25.75.-q, 25.75.Ld

One of the important results in Au+Au collisions is the large elliptic flow is non-central collisions [1, 2, 3, 4]. Large elliptic flows establish that in non-central Au+Au collisions, a collective QCD matter is created. Whether the matter can be characterized as the lattice QCD [5] predicted Quark-Gluon-Plasma (QGP) or not, is still a question of debate. Qualitatively, elliptic flow are naturally explained in hydrodynamics, rescattering of secondaries generates pressure and drives the subsequent collective motion. In non-central collisions, the reaction zone is asymmetric (almond shaped), pressure gradient is large in one direction and small in the other. The asymmetric pressure gradient generates the elliptic flow. As the fluid evolve and expands, asymmetry in the reaction zone decreases and comes a stage when reaction zone become symmetric and system no longer generate elliptic flow. Elliptic flow is early time phenomena and a sensitive probe to the early stage of the fluid.

Ideal hydrodynamics has been quite successful in explaining RHIC data on elliptic flow [6]. Assuming that the collision produces QGP, which undergoes 1st order phase transition at a critical temperature $T_c=164$ MeV, elliptic flow of identified particles are explained up to $p_T \sim 1.5$ GeV. Ideal hydrodynamics also reproduces the transverse momentum dependence of identified particles, again up to $p_T \sim 1.5$ GeV, which exhaust more than 99% of particle production. Success of *ideal* hydrodynamics in explaining bulk of the data [6], together with the string theory motivated lower limit of shear viscosity $\eta/s \geq 1/4\pi$ [7, 8] has led to a paradigm [9, 10] that in Au+Au collisions, a nearly perfect fluid is created.

However, the paradigm of *perfect fluid*, produced in Au+Au collisions at RHIC, need to be clarified. As indicated above, the ideal hydrodynamics is only partially successful and in a limited p_T range ($p_T \leq 1.5$ GeV) [11]. The transverse momentum spectra of identified particles starts to deviate from ideal fluid dynamics prediction beyond $p_T \sim 1.5$ GeV. Experimentally determined HBT radii are not reproduced in the ideal fluid dynamic models, the famous "HBT puzzle" [12]. It also does not repro-

duce the experimental trend that elliptic flow saturates at large transverse momentum. Contrary to experiment, ideal hydrodynamics predicts continually increasing elliptic flow. These shortcomings of ideal fluid dynamics indicate greater importance of non-equilibrium (dissipative) effects in the p_T ranges greater than 1.5 GeV. Indeed, saturation of elliptic flow at large p_T is a manifestation of non-equilibrium effects. In parton cascade simulations of relativistic Boltzmann equation, where dissipative effects are naturally included, elliptic flow saturates at large p_T [13]. However, parton cascade simulations do not reproduce experimental data unless the elastic parton cross-section is very high, $\sigma \sim 45$ mb. Realistic cross-sections do not generate enough flow. Recently, elliptic flow is studied in a hybrid "hydro+cascade" model [14]. In the model, initially produced QGP evolve following the ideal hydrodynamics. Just below the phase transition, a hadronic transport model is employed for the late stage evolution. The model seems to require additional dissipation at the early quark-gluon plasma phase.

Dissipation in the early QGP phase can be conveniently studied in relativistic dissipative hydrodynamics. Theories of relativistic dissipative hydrodynamics are well developed [15, 16, 17]. Problem of causality violation in 1st order theories [15, 16], are removed in the Israel-Stewart's [17] causal, 2nd order theories. Recently, there has been significant progress in numerical implementation relativistic dissipative hydrodynamics [18, 19, 20, 21, 22, 23, 24, 25, 26, 27, 28]. Elliptic flow in causal hydrodynamics has been calculated in [27, 28]. Romatschke and Romatschke [27] concluded that while data on integrated v_2 is consistent with a ratio of viscosity over entropy density up to $\eta/s \approx 0.16$, the data on minimum bias v_2 favor a much smaller viscosity, $\eta/s \approx 0.03$, lower than the ADS/CFT bound $\eta/s=0.08$. A different result was obtained in [28]. They did not compare with experiments but minimal viscosity $\eta/s=0.08$ leads to large reduction in elliptic flow compared to ideal hydrodynamics. At the Cyclotron Centre, Kolkata, we have developed a code, "AZHYDRO-KOLKATA" to solve "causal" dissipative hydrodynamics. In an earlier publication [26], we have discussed the space-time evolution of QGP fluid without any phase transition. AZHYDRO-KOLKATA results for elliptic flow (includ-

*E-mail: akc@veccal.ernet.in

ing phase transition) are presented here.

Elliptic flow of a particle (say π^-) is quantified as the 2nd harmonic of azimuthal distribution of π^- ,

$$v_2(p_T) = \frac{\int d\phi \frac{d^2 N}{dy d^2 p_T} \cos(2\phi)}{\int d\phi \frac{d^2 N}{dy d^2 p_T}}, \quad (1)$$

where $\frac{d^2 N}{dy d^2 p_T}$ is the invariant distribution of π^- . In Cooper-Frye prescription, the invariant distribution is obtained as,

$$\frac{dN}{dy d^2 p_T} = \int_{\Sigma} d\Sigma_{\mu} p^{\mu} f(x, p), \quad (2)$$

where Σ_{μ} is the freeze-out hyper surface and $f(x, p)$ is the distribution function. In viscous dynamics, the system is not in (local) equilibrium. If the system is not far from equilibrium, $f(x, p)$ can be approximated as,

$$f(x, p) = f^{(0)}(x, p)[1 + \phi(x, p)], \quad (3)$$

where $f^{(0)}(x, p)$ is the equilibrium distribution function, and $\phi(x, p) \ll 1$, is a small correction due to non-equilibrium effects. With shear viscosity as the only dissipative force the correction factor $\phi(x, p)$ can be locally approximated as,

$$\phi(x, p) = \varepsilon_{\mu\nu} p^{\mu} p^{\nu} = \frac{1}{2T^2(\varepsilon + p)} \pi_{\mu\nu} p^{\mu} p^{\nu}. \quad (4)$$

where ε, p and T are the (local) energy density, pressure and temperature. $\pi^{\mu\nu}$'s are the shear stress tensors.

Accordingly, in viscous dynamics, π^- invariant distribution has two parts,

$$\begin{aligned} \frac{dN}{dy d^2 p_T} &= \int d\Sigma_{\mu} p^{\mu} f^{(0)}(x, p) + \int d\Sigma_{\mu} p^{\mu} [f^{(0)}(x, p) \phi(x, p)] \\ &= \frac{dN^{eq}}{dy d^2 p_T} + \frac{dN^{neq}}{dy d^2 p_T}, \end{aligned} \quad (5)$$

where $\frac{dN^{neq}}{dy d^2 p_T}$ is the non-equilibrium correction to the π^- equilibrium distribution $\frac{dN^{eq}}{dy d^2 p_T}$. Since $\phi(x, p) \ll 1$ it is then necessary that $\frac{dN^{neq}}{dy d^2 p_T} \ll \frac{dN^{eq}}{dy d^2 p_T}$. Expanding Eq.1 to the 1st order,

$$\begin{aligned} v_2(p_T) &= v_2^{eq}(p_T) \\ &+ \left(-v_2^{eq} \frac{\int d\phi \frac{d^2 N^{neq}}{p_T dp_T d\phi}}{\int d\phi \frac{d^2 N^{eq}}{p_T dp_T d\phi}} + \frac{\int d\phi \cos(2\phi) \frac{d^2 N^{neq}}{p_T dp_T d\phi}}{\int d\phi \frac{d^2 N^{eq}}{p_T dp_T d\phi}} \right) \\ &= v_2^{eq}(p_T) + v_2^{corr}(p_T), \end{aligned} \quad (6)$$

where v_2^{eq} is the equilibrium elliptic flow and v_2^{corr} is the correction due to the non-equilibrium effects. Non-equilibrium correction grow quadratically with p_T (see

Eq.4). v_2^{eq} on the other hand grow less than linearly with p_T . An important conclusion can be reached from Eq.6: asymptotically, viscous hydrodynamics do not predict saturation of elliptic flow.

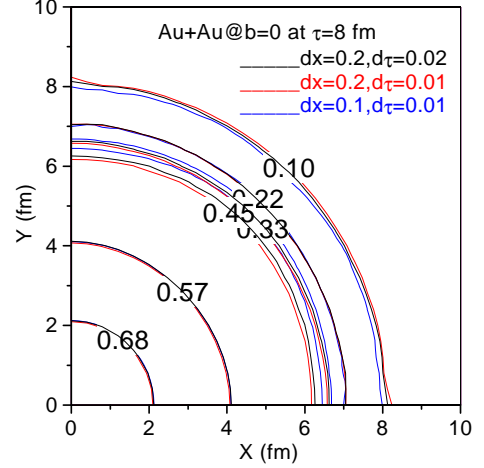


FIG. 1: (color online) constant energy density contours in $b=0$ Au+Au collisions after 8 fm of evolution.

Assuming longitudinal boost-invariance, we have solved causal dissipative hydrodynamics in 2+1 dimension. We have included the shear viscosity only. Details of equation solved and some results for space-time evolution could be found in [25]. To simulate the Au+Au collisions at RHIC, we have used the standard initial conditions described in [6]. At initial time $\tau_i=0.6$ fm, the QGP fluid was initialized with central entropy density $S_{ini} = 110 fm^{-3}$. It corresponds to peak energy density $\sim 35 GeV/fm^3$. We also use the equation of state EOS-Q described in [6], incorporating a first order phase transition at a critical temperature $T_c=164$ MeV. In viscous hydrodynamics, additionally, one has to initialize the shear stress-tensors. We assume that at initial time τ_i , shear stress-tensors have attained their boost-invariant values [25]. Viscous hydrodynamics introduces some new parameters, the viscosity coefficient η and the relaxation time τ_{relx} . Viscosity coefficient of a QGP or hadronic fluid is quite uncertain. In a strongly coupled field theory, ADS/CFT estimate gives a lower limit to shear viscosity, $\frac{\eta}{s} \geq \frac{1}{4\pi} \approx 0.08$ [7, 8]. Presently we show results for the minimal shear viscosity, $\eta/s=0.08$. For the relaxation time, we use the kinetic theory approximation for a Boltzmann gas, $\tau_{relx} = \frac{6\eta}{4p} \approx \frac{6\eta}{sT}$.

It is very important to establish the accuracy of the numerical code. Being a ratio, elliptic flow is a sensitive observable and any small error in computation can lead to large uncertainty in the elliptic flow. *Viscous hydrodynamics do not posses analytical solution against which the numerical results could be tested.* We use the general procedures to test a numerical code, (i) the results should be stable against change in integration step lengths, (ii) any symmetry in the system should not be destroyed and (iii) unphysical maxima or minima should not creep into

due to numerical error. In Fig.1, we have shown the constant energy density contours in a zero impact parameter Au+Au collisions after 8 fm of evolution. The contours are drawn for three different sets of integration step lengths, (i) $dx = dy = 0.2fm, d\tau = 0.02fm$, (the black lines) , (ii) $dx = dy = 0.2fm, d\tau = 0.01fm$, (the red lines) and (iii) $dx = dy = 0.1fm, d\tau = 0.01fm$, (the blue lines). The ratio of viscosity over entropy density is $\eta/s=0.08$. Fig.1 shows that all the three conditions mentioned above are satisfied. The evolution is stable against change in integration step lengths. In the interior of the fluid, energy density surfaces are exactly reproduced and one can not distinguish the lines for different integration step lengths. At large radius, energy density distribution does show dependence on integration step lengths but the dependence is small. For example, the spatial uncertainty in the $\epsilon=0.1$ GeV surface is less than 3-4% only. In a $b=0$ collision, initial energy density is azimuthally symmetric. The symmetry is maintained during the evolution. Also the smooth fall of energy density along the radius indicates that no new maxima or minima are generated during the evolution.

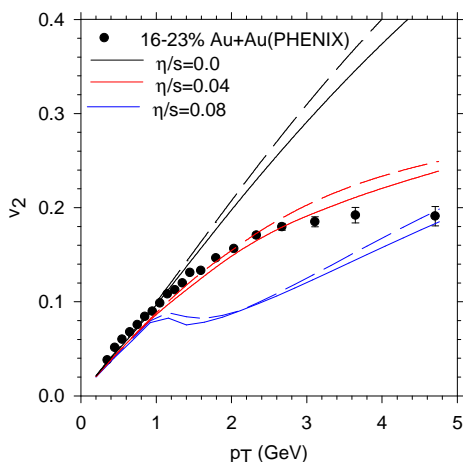


FIG. 2: (color online) The solid and dashed lines show the p_T dependence of elliptic flow in evolution with integration step lengths $dx = dy = 0.2, d\tau = 0.02$ and $dx = dy = 0.1, d\tau = 0.01$. The black lines corresponds to ideal fluid. The red and blue lines corresponds to viscous fluid with $\eta/s=0.04$ and with $\eta/s=0.08$ respectively. The filled circles are PHENIX data [29] on elliptic flow of charged particles in 16-23% Au+Au collisions.

Any dependence of the hydrodynamic evolution on integration step lengths will be reflected on the freeze-out surface and consequently on observables like particle p_T spectra, elliptic flow etc. In Fig.2, we have computed the elliptic flow for π^- in a $b=6.5$ fm Au+Au collision. The dashed and solid lines are v_2 in evolution with integration step lengths (i) $dx = dy = 0.1fm, d\tau = 0.01fm$ and (ii) $dx = dy = 0.2fm, d\tau = 0.02fm$ respectively. We have shown results both for ideal (black lines) and viscous fluid with two values of viscosity $\eta/s=0.04$ (the red lines) and 0.08 (the blue lines). The freeze-out tem-

perature is assumed to be $T_F=150$ MeV. Both in ideal and in viscous dynamics, v_2 depend marginally on integration step lengths. Elliptic flow in evolution with $dx = dy = 0.1fm, d\tau = 0.01fm$ is $\sim 10\%$ more than in evolution with $dx = dy = 0.2fm, d\tau = 0.02fm$. Elliptic flow is very sensitive observable. Stability of v_2 imply that the hydrodynamic evolution, whether computed with integration step lengths (i) $dx = dy = 0.1fm, d\tau = 0.01fm$ or (ii) $dx = dy = 0.2fm, d\tau = 0.02fm$, lead to nearly identical freeze-out surfaces.

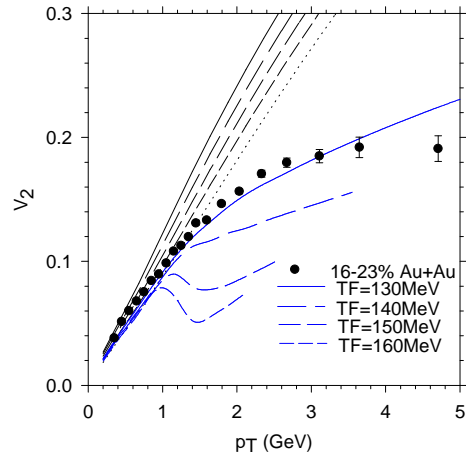


FIG. 3: p_T dependence of elliptic flow in ideal (the black lines) and in minimal viscous (the blue lines) dynamics for $T_F=130, 140, 150$ and 160 MeV in a $b=6.5$ fm Au+Au collision. The filled circles are the PHENIX data [29] on the elliptic flow in 16-23% Au+Au collisions.

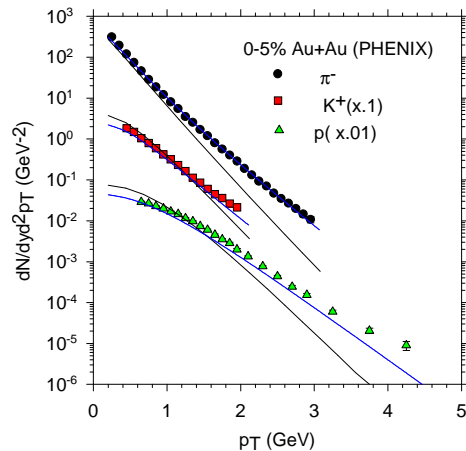


FIG. 4: PHENIX data [30] on the transverse momentum dependence π^- , K^+ and proton in 0-5% Au+Au collisions are shown. The blue and black lines are predictions from minimally viscous hydrodynamics and from ideal hydrodynamics in a $b=2.3$ fm Au+Au collision.

Effect of viscosity on elliptic flow is also evident in Fig.2. Under identical conditions elliptic flow is less in viscous dynamics than in ideal dynamics. More viscous is the fluid less is the elliptic flow. $b=6.5$ fm col-

lision roughly corresponds to 13-26% Au+Au collision. In Fig.2, PHENIX data [29] on the elliptic flow in 16-23% Au+Au collisions are shown (the filled circles). As mentioned earlier, ideal fluid dynamics fails to explain the data beyond $p_T \approx 1.5$ GeV. Data are not explained in minimally viscous dynamics also. ADS/CFT lower bound on viscosity $\eta/s=0.08$ reduce the elliptic flow more than necessary. Reduction is less for still lower viscosity and PHENIX data are well explained up to $p_T \sim 3$ GeV for viscosity $\eta/s=0.04$. A similar result is also obtained in [27]. Minimum bias STAR data seems to favor smaller viscosity ($\eta/s=0.03$), lower than the ADS/CFT bound.

In a viscous fluid, elliptic flow depend strongly on the freeze-out temperature. For the minimally viscous fluid ($\eta/s=0.08$), PHENIX data could be explained if the hadronic freeze-out occur at temperature lower than 150 MeV. The shear stress tensors will evolve for longer duration to lower values and contribute less to the non-equilibrium distribution function and to the elliptic flow. In Fig.3, the elliptic flow for freeze-out temperatures $T_F=130,140,150$ and 160 MeV are shown. Curves are drawn up to p_T such that $\frac{dN^{neq}}{dyd^2p_T} < \frac{dN^{neq}}{dyd^2p_T}$. As expected, elliptic flow increases as T_F decreases. p_T range over which viscous dynamics remain valid is also extended. For $T_F=130$ MeV, minimally viscous dynamics reproduce the PHENIX data in 16-23% Au+Au collisions, well up to $p_T=3.6$ GeV. However, viscous dynamics do not reproduce saturaton. At large p_T jets are important. Without the effect of jets accounted for, possibly saturation of elliptic flow could not be explained. For comparison,

we have also shown the elliptic flow in ideal dynamics. In ideal dynamics freeze-out dependence is comparatively less. We may mention that fit to elliptic flow data in other centrality ranges of collisions is not as good as shown in Fig.3. Minimally viscous dynamics produces less elliptic flow in very central collisions (0-5%, 5-10%) collisions. In less central collisions data are reasonably well reproduced.

Viscous hydrodynamics with minimal viscosity $\eta/s=0.08$ also reproduces the transverse momentum distribution of identified particles. In Fig.4, we have shown the PHENIX data [30] on transverse momentum distribution of π^- , K^+ and protons in 0-5% Au+Au collisions. The blue lines are viscous hydrodynamics predictions in a $b=2.3$ fm Au+Au collision. Freeze-out temperature is $T_F=130$ MeV. Minimally viscous hydrodynamics ($\eta/s=0.08$) reproduces the π^- , K^+ and proton spectra up to $p_T=3$ GeV. A comparable fit could not be obtained in ideal dynamics.

To summarise, in causal dissipative hydrodynamics, we have studied the effect of viscosity on elliptic flow. Under identical conditions, elliptic flow is less in viscous dynamics than in ideal dynamics. For minimally viscous fluid ($\eta/s=0.08$), PHENIX data on elliptic flow in 16-23% Au+Au collisions are well explained up to $p_T \approx 3.6$ GeV. This is to be contrasted with ideal dynamics which can explain the flow up to $p_T \approx 1.5$ GeV only. Minimally viscous fluid also explains the p_T spectra of π^- , K^+ and protons, much better than in ideal dynamics.

-
- [1] BRAHMS Collaboration, I. Arsene *et al.*, Nucl. Phys. A **757**, 1 (2005).
[2] PHOBOS Collaboration, B. B. Back *et al.*, Nucl. Phys. A **757**, 28 (2005).
[3] PHENIX Collaboration, K. Adcox *et al.*, Nucl. Phys. A **757** 184 (2005).
[4] STAR Collaboration, J. Adams *et al.*, Nucl. Phys. A **757** 102 (2005).
[5] Karsch F, Laermann E, Petreczky P, Stickan S and Wetzorke I, 2001 *Proceedings of NIC Symposium* (Ed. H. Rollnik and D. Wolf, John von Neumann Institute for Computing, Jülich, NIC Series, vol.9, ISBN 3-00-009055-X, pp.173-82,2002.)
[6] P. F. Kolb and U. Heinz, in *Quark-Gluon Plasma 3*, edited by R. C. Hwa and X.-N. Wang (World Scientific, Singapore, 2004), p. 634.
[7] G. Policastro, D. T. Son and A. O. Starinets, Phys. Rev. Lett. **87**, 081601 (2001).
[8] G. Policastro, D. T. Son and A. O. Starinets, JHEP **0209**, 043 (2002).
[9] E. Shuryak, Prog. Part. Nucl. Phys. **53**, 273 (2004)
[10] U. W. Heinz, arXiv:nucl-th/0512051.
[11] U. Heinz, J. Phys. G **31**, S717 (2005).
[12] U. W. Heinz and P. F. Kolb, arXiv:hep-ph/0204061.
[13] D. Molnar and M. Gyulassy, Nucl. Phys. A **697**, 495 (2002) [Erratum-ibid. A **703**, 893 (2002)].
[14] T. Hirano, U. W. Heinz, D. Kharzeev, R. Lacey and Y. Nara, Phys. Lett. B **636**, 299 (2006).
[15] C. Eckart, Phys. Rev. **58**, 919 (1940).
[16] L. D. Landau and E. M. Lifshitz, *Fluid Mechanics*, Sect. 127, Pergamon, Oxford, 1963.
[17] W. Israel, Ann. Phys. (N.Y.) **100**, 310 (1976); W. Israel and J. M. Stewart, Ann. Phys. (N.Y.) **118**, 349 (1979).
[18] D. Teaney, Phys. Rev. C **68**, 034913 (2003) [arXiv:nucl-th/0301099].
[19] D. A. Teaney, J. Phys. G **30**, S1247 (2004).
[20] A. Muronga and D. H. Rischke, nucl-th/0407114 (v2).
[21] T. Koide, G. S. Denicol, Ph. Mota and T. Kodama, Phys. Rev. C **75**, 034909 (2007).
[22] R. Baier and P. Romatschke, arXiv:nucl-th/0610108.
[23] A. K. Chaudhuri and U. W. Heinz, J. Phys. Conf. Ser. **50**, 251 (2006).
[24] U. W. Heinz, H. Song and A. K. Chaudhuri, Phys. Rev. C **73**, 034904 (2006).
[25] A. K. Chaudhuri, Phys. Rev. C **74**, 044904 (2006). arXiv:nucl-th/0703027; arXiv:nucl-th/0703029;
[26] A. K. Chaudhuri, arXiv:0704.0134 [nucl-th].
[27] P. Romatschke and U. Romatschke, arXiv:0706.1522 [nucl-th].
[28] H. Song and U. W. Heinz, arXiv:0709.0742 [nucl-th].
[29] S. S. Adler *et al.* [PHENIX Collaboration], Phys. Rev. Lett. **94**, 232302 (2005).
[30] S. S. Adler *et al.* [PHENIX Collaboration], Phys. Rev. C **69**, 034909 (2004) [arXiv:nucl-ex/0307022].